Chemical Science

ROYAL SOCIETY OF CHEMISTRY

EDGE ARTICLE

View Article Online
View Journal | View Issue

Cite this: *Chem. Sci.*, 2025, **16**, 7249

All publication charges for this article have been paid for by the Royal Society of Chemistry

Vacuum infiltration for priming of soybean seeds: optimization and particle tracking using fluorescent silica nanoparticles†

Tana L. O'Keefe, ‡[a] Beza Tuga, ‡[a] Chaoyi Deng, [b] Sharmaka Mohamud,[a] Rima Jamous,[a] Mark A. Sanders, [c] Wade H. Elmer,[b] Jason C. White [b] and Christy L. Haynes *[a]

Received 18th December 2024
Accepted 3rd March 2025

DOI: 10.1039/d4sc08566c

rsc.li/chemical-science

Agrochemical delivery is highly inefficient, and novel application methods are necessary to promote crop health and yields while reducing environmental impact. In this work, a vacuum infiltration seed priming strategy was developed to incorporate silica nanoparticles into soybeans. Although successful in initial greenhouse and field studies, little is known about the amount of nutrient being delivered and the conditions for optimum accumulation. Herein, various infiltration conditions were evaluated using fluorescent silica nanoparticles and confocal microscopy, including nanoparticle surface charge and concentration, infiltration time, infiltrate ionic strength and pH, and seed presoaking. Negative nanoparticle surface charge, higher nanoparticle concentration, shorter infiltration time, and potassium-based salts resulted in greater nanoparticle infiltration. Seed coat elemental analysis complemented fluorescence data and highlighted the co-delivery of beneficial macronutrients including potassium and magnesium under ionic salt infiltration conditions. Overall, these findings illustrate a new strategy to biofortify nanoscale nutrients into soybean seeds that can be expanded into other agrochemical targets and crop species to promote sustainable agriculture.

Introduction

Of the Sustainable Development Goals outlined by the United Nations in 2015, Goal #2, eradicating world hunger, continues to be a problem that is increasingly challenged by global population growth, climate change, and the COVID-19 pandemic.[1] Furthermore, the rate of agricultural yield increase continues to decline, resulting in less available food to feed the growing population.[2] In the last century, it is clear that the application of fertilizers and agrochemicals has played a substantial role towards improving global food production as today, more than 50% of the crops feeding the world are grown on synthetic nitrogen (N) fertilizers to enhance crop health and yields.[3] Despite this clear benefit, a significant portion of the applied agrochemicals are not taken up by plants, resulting in a usage efficiency as low as 40% globally.[4] Today, agriculture heavily relies on traditional application methods, such as foliar spray or soil treatments; however, these methods are highly inefficient, with anywhere from 10–75% of the applied agrochemicals not reaching their desired targets.[2,5,6] This inefficiency often leads to repeated application or overapplication of agrochemicals. Specifically, in the case of N fertilizers, 50–70% of applied nitrogen is lost to volatilization, leaching, and degradation processes. This allows various forms of N, such as ammonia (NH_3) and nitrous oxide (N_2O), to enter the environment, causing negative agronomic, environmental, and human health impacts.[7] These negative impacts include increased greenhouse gas emissions, ozone degradation, water pollution, and changes to biodiversity.[7,8] As poor and inefficient application methods, such as spray or soil treatments, contribute to significant agrochemical loss, innovative approaches towards developing simple, rapid, and cost-effective application methods are needed to reduce the aforementioned negative consequences of applied agrochemicals.

One such alternative involves seed treatments. For instance, seed priming involves the hydration of seeds with a treatment of interest to the point of pre-germination, followed by the drying of the seeds prior to planting.[9] This process allows seeds to progress through the initial stage of germination, enabling faster and more uniform emergence when planted.[9] Previously, seed priming treatments have been investigated in several plant systems using water,[10] plant regulators (*e.g.* jasmonic acid),[11]

[a]*Department of Chemistry, University of Minnesota – Twin Cities, Minneapolis, MN, 55455, USA. E-mail: chaynes@umn.edu*

[b]*The Connecticut Agricultural Experiment Station, New Haven, Connecticut 06511, USA*

[c]*University Imaging Centers, University of Minnesota – Twin Cities, Minneapolis, MN, 55455, USA*

† Electronic supplementary information (ESI) available. See DOI: https://doi.org/10.1039/d4sc08566c

‡ Denotes co-authorship.

nutrients,[12–15] and fertilizers.[16] Plants grown from priming treatments have shown increased germination rates, increased abiotic and biotic stress resistance, and increased crop production.[9,17] Furthermore, nanoparticles (NPs), materials that have at least one dimension less than 100 nm, have shown great promise as new agricultural technologies and are also used as seed priming agents.[18,19] Seed coating is another strategy that involves applying the desired treatment to the external surface of seeds, and recent work has investigated the used of NP-based seed coatings.[20] For example, Abeywardana *et al.* coated maize (*Zea mays*) seeds with zinc-doped urea–hydroxyapatite nanohybrids to deliver both macro (nitrogen and phosphorous) and micro (zinc) nutrients.[21] Their seed coating increased the growth of maize by ~69% and improved germination rate by ~19%.[21] Zinc oxide NPs were also used as a coating for wheat (*Triticum aestivum*) seeds by Elhaj Baddar *et al.*,[22] promoting higher Zn accumulation in wheat grain compared to soil amendments, making them a great alternative to soil fertilizers. Furthermore, nanofibers were employed in a seed coating by Xu *et al.* as a copper-based delivery agent to tomato and lettuce seeds in both healthy and diseased conditions.[23] Greenhouse studies revealed increased germination rates, particularly in diseased conditions.[23] While seed treatments have obvious benefits, both seed priming and coating come with certain limitations. The seed priming process results in uncontrolled water uptake that could result in unwanted germination of the seeds prior to planting and reduces the shelf life of seeds. Additionally, storage conditions of seeds (humidity, temperature) after priming can negatively impact their viability.[9] Seed coatings, on the other hand, only incorporate the treatment onto the outside of the seed, and some coating techniques require special instrumentation and expensive raw materials, making the large scale application a costly hurdle.[20] Thus, this work demonstrates the utility of a novel vacuum infiltration method that has the potential to overcome these limitations by (i) treating seeds under vacuum to incorporate treatments further into the seed and (ii) conducting treatments at shorter time scales where the risk of accidental seed germination is greatly reduced. This method was tested using soybeans (*Glycine max*) as a plant model.

Soybean (*Glycine max*) is among the top-produced crops in the world, with over 372 million tons being produced globally in 2021,[24] making them a high protein crop that could play a significant role in achieving global food security. Additionally, soybean seeds form symbiotic relationships with soil bacteria to perform biological nitrogen fixation, allowing soybeans to play a significant role in our ecosystem.[25] However, this crop, like most others, heavily relies on fertilizers and other agrochemicals for growth and crop yield, and as already mentioned, this agrochemical delivery process is highly inefficient. Soybean seed morphology has two main components: a seed coat and embryo (Fig. 1).[27] As the outermost layer, and first point of contact, the seed coat is a crucial parameter to consider for seed treatments. The soybean seed coats contain similar seed coat characteristics to other legumes with 3 distinct regions: an epidermal layer, a sub-epidermal layer, and a few layers of inner parenchyma tissue, all of which account for 4–6% of the total

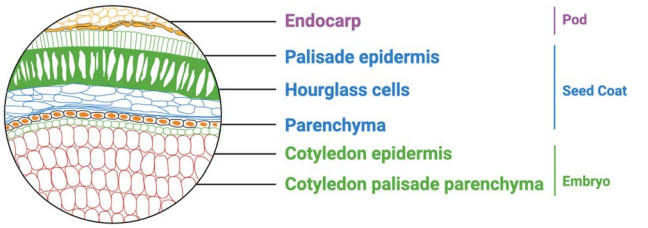

Fig. 1 Soybean seed morphology highlighting the pod, seed coat and embryo of a soybean seed. The seed coat contains hourglass cells that are air-filled and targeted by vacuum infiltration. Adapted from ref. 26 with permission Canadian Science Publishing, copyright 2008. Figure created in https://www.biorender.com/.

individual seed weight.[26,27] An interesting feature of mature soybeans seed coats is the presence of hourglass cells (or osteosclereids) within the sub-epidermal layer which are known for their significant air spaces between cells.[28] Vacuum infiltration targets those air spaces to allow for efficient delivery of various treatments into seeds. More specifically, after being placed in a suspension of the desired treatment under vacuum, this method relies on the removal of air from the air pockets, allowing for the intracellular air pockets to backfill with the treatment of choice upon vacuum release, thereby targeting the hourglass cells within the seed coat (Fig. 2a). Herein, we are focused on optimizing this vacuum infiltration method to deliver nanoparticles (NPs) as the treatment of interest. With the development of new agricultural technologies to increase food production, NPs are showing promise towards improving agrochemical delivery, and in turn, plant disease suppression and crop yield in a variety of crops.[29–31] The control over NP characteristics such as size, surface charge,[32] shape,[33] surface modifications,[34] dissolution and other transformations[35,36] allows for their improved efficacy at lower doses when compared to conventional agrochemical formulations.[37] In particular, mesoporous silica NPs have drawn attention for agricultural applications due to their sustainability, easy tunability, biocompatibility, and ability to load and release agrochemicals or other cargo.[38,39] Their ability to transform and release silicic acid is responsible for their success in plant studies due to the benefits of silicic acid increasing plant stress tolerance. Furthermore, the synthetic flexibility of these silica NPs allows for the incorporation of fluorescent dyes, such as fluorescein isothiocyanate (FITC) or rhodamine B isothiocyanate (RITC), permitting the efficient tracking of NPs within plants which is key to mechanistic understandings of their uptake and mode of actions. The infiltration trends revealed with fluorescent silica nanoparticles in this work can be used in future work where the nanoparticles of interest are not easy to track and quantify.

A limited number of studies have employed vacuum infiltration as a seed treatment and fortification strategy in greenhouse and field studies. Buchman *et al.* vacuum infiltrated mesoporous silica NPs into watermelon (*Citrullus lanatus*) seeds, which were then followed by a foliar dip application of the NP suspension, prior to greenhouse and field studies.[34] This method resulted in a ~27–40% reduction in watermelon

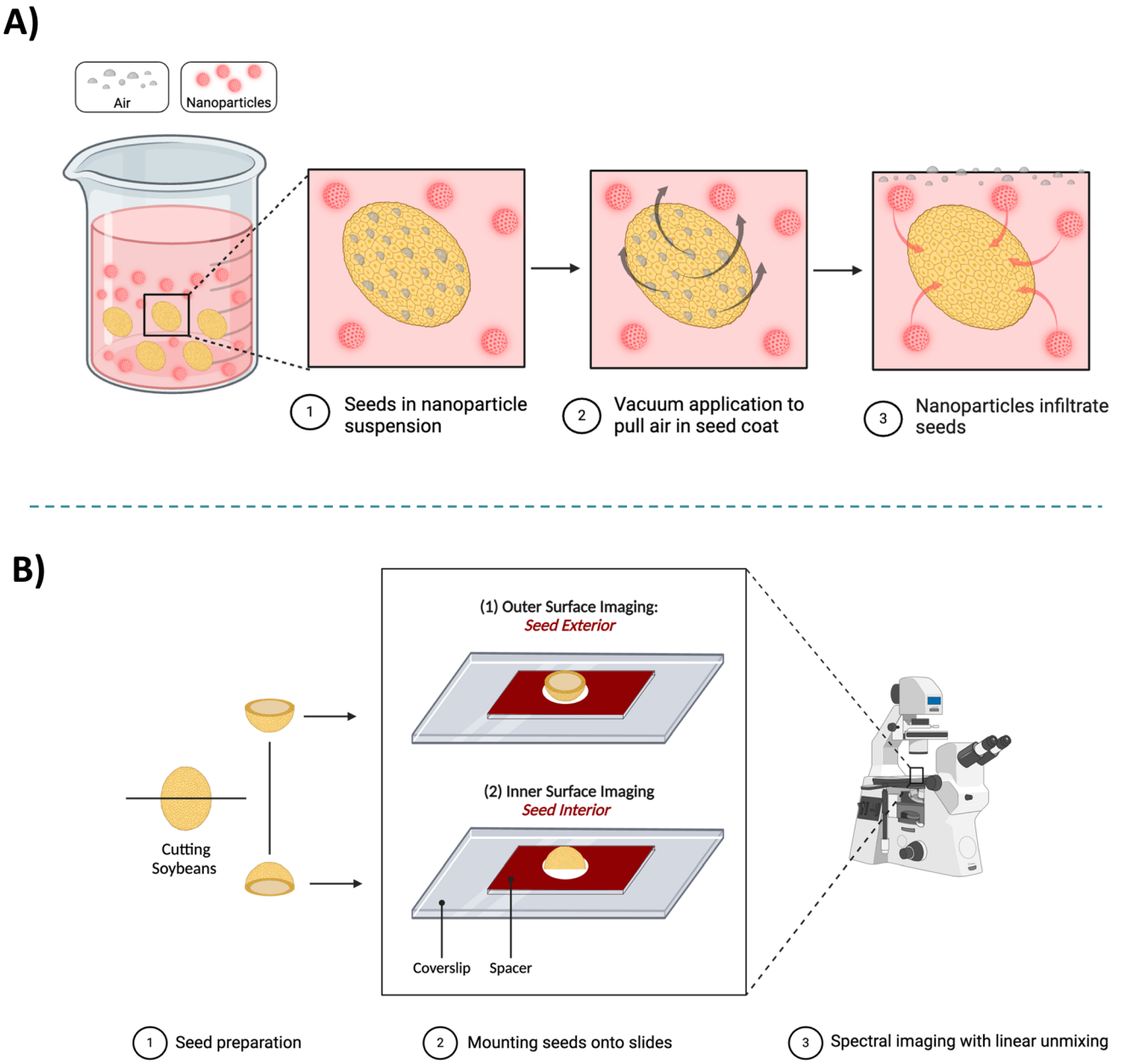

Fig. 2 (A) Vacuum infiltration process where vacuum application removes air from seed coat and allows for nanoparticle incorporation into soybean seeds. (B) Seed and slide preparation for confocal microscopy. Figure created in https://www.biorender.com/.

disease in the greenhouse studies and a 70% increase in disease-free plant yield in the field. O'Keefe *et al.* subsequently compared foliar application to vacuum infiltration of the same mesoporous silica NPs with soybean.[40] The seed treatment proved to be more effective than foliar application, with a single seed treatment reducing disease severity (*Fusarium* fungal infection) by 30% in the greenhouse and 12–15% in the field. Despite the success in these seed treatments towards disease suppression and increased crop health and yield, much remains unknown about the vacuum infiltration method in the context of how much NP is being incorporated into the seeds, how they distribute within the seed, and what conditions are ideal for improved nanoscale nutrient fortification.

Overall, this is the first study to systematically evaluate vacuum infiltration of silica nanoparticles for a simpler, safer, and more efficient delivery method for nanoscale nutrients. While this work focuses on soybean seeds, similarity in seed physiology across crop species suggests that the optimized conditions are likely generalizable, or at least a reasonable starting point, for other crop species.

Methods

Materials

Cetyltrimethylammonium bromide (CTAB), *N*,*N*-dimethylhexadecylamine (DMHA), chlorotrimethyl silane, tetraethylorthosilicate (TEOS), (3-aminopropyl)triethoxysilane (APTES),

rhodamine B isothiocyanate (RITC), magnesium nitrate, and magnesium sulfate were obtained from Sigma-Aldrich (St. Louis, MO). Ammonium hydroxide (28–30%) was purchased from Avantor Performance Materials (Center Valley, PA). Potassium nitrate, potassium sulfate, and sodium hydroxide were obtained from Fisher Scientific (Waltham, MA). Soybean seeds (*Glycine max*) were purchased from Jonny's selected seeds (Winslow, ME). All chemicals were used as received without further purification.

RITC-UMN synthesis

To synthesize RITC-UMNs, a previously reported procedure for making fluorescent mesoporous silica nanoparticles was adapted.[41] First, RITC (2.14 mg) was dissolved in 200 proof ethanol (4 mL). Then, 8 mL of (3-aminopropyl)triethoxysilane (APTES) was added, and the solution was stirred in the dark for 18 h at room temperature before use. This produces a RITC silane that can be incorporated directly into the silica network by co-condensation with the silica precursor, TEOS.

RITC-UMNs were synthesized *via* the sol–gel method as previously reported.[42] Briefly, 0.1450 g of cetyltrimethylammonium bromide (CTAB) was mixed with 10 mL of Milli-Q water, 150 μL *N*,*N*-dimethylhexadecylamine (DMHA), and 116 μL of decane. The solution was stirred for 1 h at 50 °C and 700 rpm. The mixture was then sonicated for 1.5 h in a sonication bath to increase micelle formation. Simultaneously, 150 g of 0.256 M NH_4OH in an Erlenmeyer flask were heated to 50 °C and stirred at 300 rpm. After sonication, the micelle solution was transferred to the Erlenmeyer flask containing NH_4OH. Next, 2.5 mL of 0.88 M ethanolic tetraethyl orthosilicate (TEOS) and 1 mL of the RITC solution was added dropwise *via* an addition funnel, and the solution was allowed to react for 1 h at 50 °C and 700 rpm. The UMN surface was then functionalized by adding 450 μL of 2-[methoxy(polyethyleneoxy)-propyl]$_{6-9}$-trimethoxysilane dropwise. The solution was stirred for 30 min at 50 °C and 700 rpm before adding 68 μL of TMS and allowed to age overnight. After aging, the solution was transferred to a glass media bottle and hydrothermally treated in a 90 °C oven for 24 h. Following hydrothermal treatment, the suspension of RITC-UMNs was removed from the oven, filtered using a Buchner funnel, and the filtrate was transferred to centrifuge tubes. The nanoparticles were centrifuged (Beckman Coulter Optima L) at 66 000×*g*, under vacuum, at 4 °C for 35 min. The supernatant was removed, and the pellet was re-dispersed in NH_4NO_3 to perform an ion exchange reaction to remove the surfactant, CTAB. The suspension was stirred under reflux for 1 h at 50 °C before centrifuging and washing with 190 proof ethanol. Another reflux step using NH_4NO_3 was carried out, followed by several washing steps with ethanol. Upon the final centrifugation, the UMNs were re-dispersed in 200 proof ethanol.

APTES-modified RITC-UMN synthesis

APTES-modified RITC-UMNs were synthesized in a similar manner as above. However, 30 min after the addition of TMS, 184 μL of APTES was added to incorporate amine functionality and positive charge to the surface. This solution was allowed to stir for an additional 24 h before proceeding with the hydrothermal treatment and purification as outlined above.

Dynamic light scattering and zeta potential measurements

The RITC-UMNs and APTES-modified RITC-UMNs were diluted to approximately 1 mg mL^{-1} in Milli-Q water after drying by rotary evaporator for dynamic light scattering (DLS) and ζ-potential measurements. The RITC-UMN suspensions were sonicated for 10 minutes prior to measurement to ensure full dispersion. Both measurements were performed using a Malvern Zetasizer Pro instrument (Westborough, MA). Values for hydrodynamic diameter and zeta potential were recorded from 3 material replicates that also included 3 technical replicates.

N_2 physisorption

After purification, the RITC-UMN samples were dried by rotary evaporator at 10 torr for 1 hour. The nitrogen physisorption glassware was weighed three times, and the dried sample (∼60 mg) was transferred into the sample tube. The sample was degassed on the Micromeritics ASAP 2020 surface area and porosity analyzer (Norcross, GA) for 5 h at 150 °C under high vacuum. The glassware and degassed sample were removed from the instrument and weighed three times to calculate the average sample mass of dried particles. The sample was then analyzed at cryogenic temperature using the analysis port. The surface area and pore volume were determined using the Barrett–Joyner–Halenda (BJH) method.

Transmission electron microscopy (TEM)

To prepare RITC-UMNs for TEM imaging, the particles were diluted to approximately 0.5 mg mL^{-1} in ethanol and sonicated for 10 minutes before sample preparation. Then, 200 mesh copper grids with Formvar and carbon supports (Ted Pella, Inc.) were dipped in the suspension and dried for 30 seconds at 65 °C. TEM images were acquired using a Thermo Fisher Talos F200x G2 at an acceleration voltage of 200 keV with a Thermo Fisher Ceta camera.

Fluorescence measurements

Fluorescence measurements were performed on a Horiba PTI QM-400 fluorometer (Irvine, CA); the nanoparticle suspensions (∼1 mg mL^{-1} in ethanol) were excited at 560 nm to collect the corresponding steady-state emission.

Preparation of different ionic strength and pH solutions

Solutions of KNO_3, K_2SO_4, $Mg(NO_3)_2$, and $MgSO_4$ were prepared in 500 mL volumetric flasks to obtain ionic strengths of 40 and 200 mM. For KNO_3, solutions with an ionic strength of 10 mM and 50 mM were also prepared to allow for concentration comparisons to the other solutions in addition to the 40 mM and 200 mM comparisons. To prepare the solutions with varying pH, the pH of water was adjusted using 0.01 M NaOH to values of 6, 6.5, 7, and 7.5.

Vacuum infiltration of soybean seeds

Six soybean (*Glycine max*) seeds were placed in 30 mL of the desired treatment suspension in a 50 mL beaker, and the beakers were transferred to a vacuum desiccator. A vacuum was applied to reach −0.1 MPa, and the seeds were under pressure for 10, 20, or 30 minutes. The vacuum was slowly released after the vacuum infiltration time was reached. The beakers were then removed from the desiccator, suspensions were decanted, and the soybean seeds were placed into small Petri dishes for 24 h to dry. After 24 h, a razorblade was used to slice the seeds in half, and sliced seeds were stored in epitubes until imaging.

Confocal microscopy and image analysis

Prior to imaging, two layers of Press-to-Seal silicone spacers (Thermo Fisher) with $\frac{3}{8}$ inch-diameter-holes were attached to no. 1.5 coverslips. Half of the seeds were placed inside the holes while allowing for the seed coat to come into contact with the coverslip (Fig. 2b). DL immersion oil was added to optimize refractive index and to stabilize the sample within the spacer.

The exterior of the half seed was imaged with a 10× objective (0.45 NA, PlanApo, WD 4 mm) using excitation wavelengths of 405, 488, 561, and 640 nm on a Nikon A1Rsi confocal microscope (Tokyo, Japan) with a 32-channel spectral detector. Spectral images were acquired with a bandwidth of 6 nm, spanning a range of 564 nm to 742 nm, to generate a lambda stack of 32 images.

Spectral images were unmixed using a linear unmixing algorithm on Nikon Elements (vers. 6.02.01) using fluorescence spectra of RITC-UMNs and APTES-modified RITC-UMNs. Once unmixed, images were processed and analyzed in FIJI (Fig. S1†). Upon opening the images in FIJI, the RITC channel was thresholded using percentile thresholding. Then, the wand tool was used to select a region of interest (ROI) that has the same intensity reading around the entire outside of the seed. The image was duplicated to zoom in on the ROI, and the ROI was left in place. The duplicate image was thresholded with moments thresholding. A measurement was taken, and the average intensity over the area of the ROI was recorded. The measurement also recorded the area and standard deviation, as well as the minimum and maximum threshold. Triplicate seed measurements were recorded for each condition tested. The values were averaged and plotted in GraphPad Prism for further analysis. Additionally, the seeds were inverted to place the seed interior in contact with the microscope coverslip and at the imaging plane. Similar imaging was performed; the edge of the seed was first identified based on bright field and fluorescent visualization before moving away from the edge to obtain an image of the seed interior (embryo). The seed interior was assumed to be relatively homogenous and that the selected image area was representative of that homogeneity. Unmixing was performed as described above; the unmixed images were thresholded using moments thresholding, and the average intensity was recorded for the entire image for triplicate seed measurements. To ensure consistency, only seeds that were processed in the same infiltration were compared to each other for image analysis.

Soybean seed coat elemental content

The content of silicon, potassium, magnesium and sulfur in seeds that were vacuum infiltrated for 10 minutes with RITC-UMNs at 500 mg L^{-1} in water, 50 mM KNO_3, 200 mM KNO_3, K_2SO_4, $Mg_2(NO)_3$, or $MgSO_4$ was measured using inductively coupled plasma optical emission spectroscopy (ICP-OES). The elemental content in seeds treated with salt controls with no nanoparticle present was also measured. Specifically, following infiltration, seed coats were separated from the embryo and dried in air for 48 h. For a single measurement, seed coats from 12 different seeds were combined to attain the required mass for ICP-OES. Dried plant tissue samples were weighed and digested in digestion tubes with 5 mL of plasma-pure nitric acid (HNO_3; Fisher Scientific, Massachusetts). The digestion process was conducted at 115 °C for 45 minutes using a hot block (DigiPREP MS, SCP SCIENCE, Quebec City, Canada). After digestion, the samples were diluted to a final volume of 50 mL using deionized water. Elemental analysis of macronutrients and micronutrients was performed using ICP-OES (iCAP 6500, Thermo Fisher Scientific, Massachusetts). To ensure quality assurance and quality control (QA/QC), blanks (no plant tissue), Si-spiked samples (1, 5, 10, and 50 mg Si/kg SiO_2 powder), and certified reference materials (NIST SRM 1570a and 1547, New Jersey) were included in the analysis. Yttrium was used as an internal standard, and a continuing calibration verification (CCV) sample containing 1 ppm Si was analyzed every 25 samples to maintain analytical precision. Element recovery rates were within the acceptable range of 85–115%.

Soybean seed germination

Soybean seeds were vacuum-infiltrated with negatively-charged RITC-UMNs and positively-charged APTES RITC-UMNs for 10 minutes at 500 mg L^{-1} in water. A no vacuum control treatment, referred to as seed priming, was also conducted at the same conditions. Seeds were then germinated using the wet paper towel germination test.[43] Ten seeds were placed between two paper towels that were moistened with water. The paper towel was rolled and placed in a sealed plastic container to retain moisture, and containers were stored at ambient temperature. Seed biomass and radicle length were measured every 3 days.

Statistical analysis

For RITC-UMN and APTES-modified RITC-UMN characterization comparisons, the mean and standard deviation for three material replicates is reported, and unpaired *t*-tests ($p < 0.05$) were used to determine statistical significance. For the initial vacuum infiltration study where infiltration time and RITC-UMN concentration were investigated, statistical analysis was performed using a two-way ANOVA with Tukey's multiple comparisons test ($p < 0.05$). For the remainder of conditions tested, a one-way ANOVA with Dunnett's multiple comparisons ($p < 0.05$) was used to determine statistical significance unless otherwise stated.

Results and discussion

Characterization of RITC-UMNs and APTES-modified RITC-UMNs

TEM was used to analyze the structure of negatively-charged RITC-UMNs and positively-charged APTES-modified RITC-UMNs (Fig. 3a and b). RITC was chosen as the fluorophore of interest, over FITC, since the fluorescence signal from nanoparticles modified with RITC have minimal overlap with chlorophyll a. As RITC is incorporated directly into the UMN framework using a co-condensation method, it allows for the stable incorporation of the fluorophore into the nanoparticle while avoiding any change to the physico-chemical nanoparticle properties. Both nanoparticles are spherical as expected. Additionally, there is mass-thickness contrast between the internal pore and the edges of the of the UMNs, indicating that there is silica network in the center with a thicker silica shell on the edges. For APTES-modified RITC-UMNs, the mass-thickness contrast is less evident, and the silica shell appears to be thicker; this is likely due to the additional modification with APTES. Dynamic light scattering was used to assess the hydrodynamic size of the nanoparticles (Fig. 3c). The APTES-modified RITC-UMNs have a statistically larger hydrodynamic diameter (148 ± 4 nm) when compared to the RITC-UMNs (121 ± 10 nm). This increase in size is again due to the extra modification and addition of APTES to the RITC-UMN surface. For RITC-UMNs, the ζ-potential is -22 ± 2 mV, while APTES-modified RITC-UMNs have a ζ-potential of $+46 \pm 7$ mV; this is a statistically significant difference (Fig. 3d) that is expected as the addition of APTES adds amine functionality to the RITC-UMN surface, creating a positive surface charge. It should be noted that the ζ-potential values also indicate that both of the RITC-UMN NPs are colloidally stable in suspension. Fluorescence spectra were measured and produced a maximum emission intensity at approximately 580 nm for both RITC-UMNs and APTES-modified RITC-UMNs (Fig. 3e). This agrees with the RITC reference spectra and previous literature for RITC-silica NPs,[44] revealing that the molecular structure of RITC is not significantly impacted by incorporation into the silica structure. Nitrogen physisorption was also performed to assess differences in the surface area and pore volume between RITC-UMNs and APTES-modified RITC-UMNs (Fig. S2†). A significant decrease in surface area was observed upon APTES modification and is likely due to APTES modification narrowing some of the mesopores and decreasing the N_2-accessible surface area. However, the pore volume of APTES-modified RITC-UMNs is the same as that of RITC-UMNs.

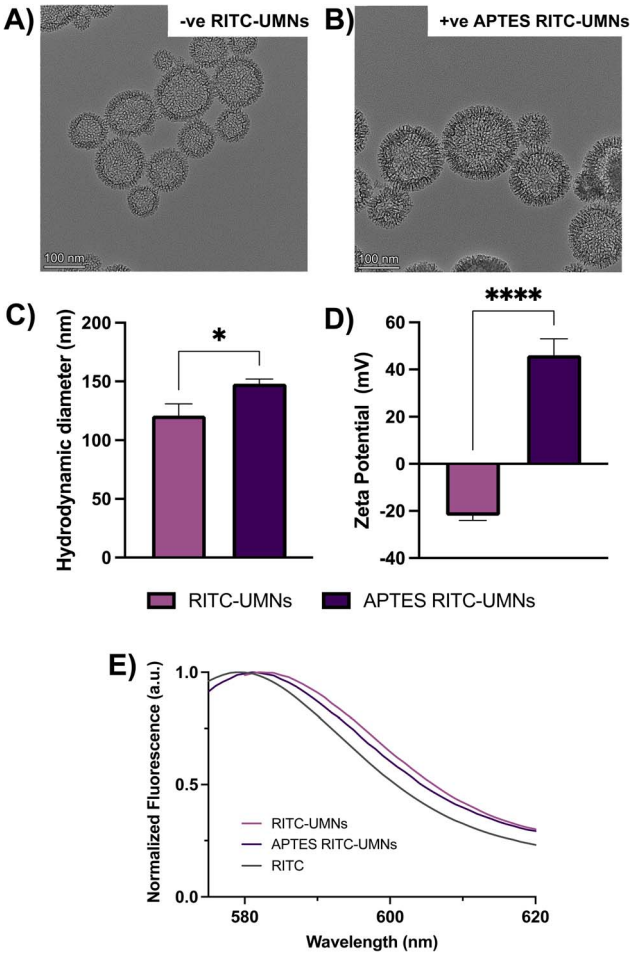

Fig. 3 Representative transmission electron micrographs of (A) RITC-UMNs and (B) APTES RITC-UMNs. (C) Hydrodynamic diameter and (D) ζ-potential of RITC-UMNs and APTES RITC-UMNs. Error bars represent the standard deviation of 3 material replicates. (E) Fluorescence emission spectra of RITC-UMNs, APTES RITC-UMNs, and RITC alone. Unpaired *t*-tests were used to evaluate statistical significance (*p < 0.05, ****p < 0.0001).

Vacuum infiltration and seed priming comparison

Conventional leaf applications of agrochemicals are inherently inefficient due to the significant loss of product that is caused by chemical volatilization or foliar runoff. Additionally, with directly spraying agrochemicals, or nanoparticles, onto mature plants comes the risk of introducing chemicals into the food chain. However, new seed treatment strategies, like vacuum infiltration, can help mitigate this effect due to the fact that as the seed grows into a mature plant and gains significant biomass, any seed treatment that was applied at the start will be effectively diluted. Furthermore, a previous study led by Buchman *et al.* determined that when silica nanoparticles were applied to watermelon seeds using vacuum infiltration, there was no evidence of silica nanoparticles present in the edible tissue of watermelon, indicating that the risk of nanoparticles entering the food chain is minimal.[34] This exciting result prompted our study to further understand vacuum infiltration and compare it with conventional seed treatment strategies like seed priming. The vacuum infiltration process is shown in Fig. 2a. Briefly, seeds are placed in a nanoparticle suspension, and a vacuum is applied to remove air from the air pockets on and within the seed coat. This allows for the incorporation of nanoparticles into the seed coat and perhaps, deeper into the seed embryo. Seeds are then sliced in half for confocal imaging, and the mean fluorescence intensity was then used as a measure of nanoparticle infiltration. Vacuum infiltration was

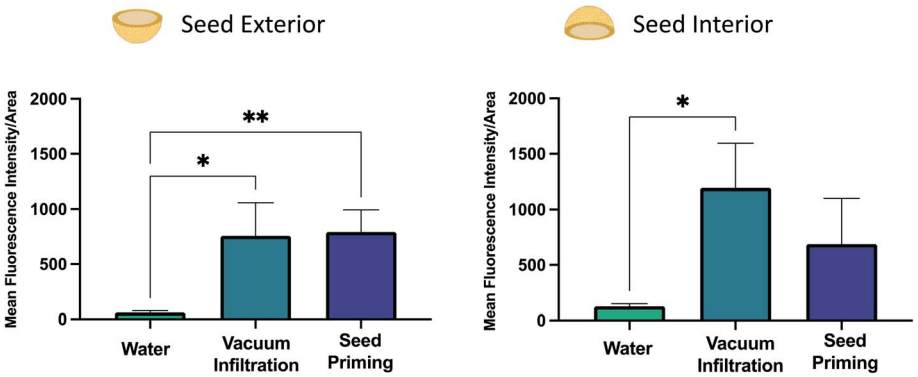

Fig. 4 Comparison of vacuum infiltration with conventional seed priming for the seed exterior (left) and seed interior (right) of negatively-charged RITC-UMNs. Error bars represent standard deviation of three seed replicates. A one-way ANOVA with Dunnett's multiple comparisons test was used to evaluate statistical significance (*$p < 0.05$, **$p < 0.01$). Soybean icon created in https://www.biorender.com/.

first compared to a common conventional method of treating seeds known as seed priming, which is similar to vacuum application but lacks the vacuum application. The mean fluorescence response for the exterior and interior of soybean seeds that were vacuum infiltrated or primed is shown in Fig. 4. The seed exteriors had similar fluorescence readouts with 750 ± 300 a.u. and 790 ± 200 a.u for vacuum infiltrated and seed priming, respectively. Previously, NP incorporation into the interior and exterior of the seed through seed priming treatments has been shown for Ag NPs in watermelon (*Citrullus lanatus*).[45] Due to the large water uptake by the soybean seeds, it is not surprising that some RITC-UMNs are incorporated into the exterior of the seed through conventional priming. However, the seed interior had a higher fluorescence readout for the vacuum infiltrated seeds with 1190 ± 400 a.u, compared to 690 ± 410 a.u for the conventional priming treatment, although the large variation precluded statistical significance. This suggests that applying a vacuum during infiltration may result in more RITC-UMN incorporation deeper into the seed embryo, offering a potentially significant competitive advantage over conventional seed treatment strategies. Following this, various conditions for vacuum infiltration such as ionic strengths, suspension pH, nanoparticle concentration, infiltration time and seed pre-soaking were tested to optimize this process for RITC-UMNs. The specific parameters are outlined in Table 1.

Vacuum infiltration time and nanoparticle concentration

First, the vacuum infiltration time and nanoparticle concentration were investigated for both negatively-charged RITC-UMNs and positively-charged APTES-modified RITC-UMNs to determine the best concentration and time for further optimization, as well as to evaluate the effect of nanoparticle surface charge on seed exterior measurements. For negatively-charged RITC-UMNs (Fig. 5a), there is a dose-dependent increase in fluorescence intensity for nanoparticles infiltrated for 10 and 30 minutes. Conversely, positively-charged APTES-modified RITC-UMNs (Fig. 5b) did not show any changes in fluorescence when compared to controls, indicating that positively-charged nanoparticles are not infiltrating effectively. The soybean seed coat is largely comprised of carbohydrates (hemicellulose, cellulose, and pectin) that contain carbonyl and hydroxyl groups,[28] so it is somewhat unexpected for negatively-charged RITC-UMNs to outperform the positively-charged nanoparticles. Furthermore, these results contradict previous trends reported for uptake of NPs in plant leaves[32,46,47] that have an analogous cuticle and palisade cell structure as the soybean seed coat. However, much remains unknown about how vacuum infiltration impacts the biochemistry on the outside surface of the seed coat. Importantly, vacuum application does have an impact on the nanoparticle characteristics, and this phenomenon is explored in a later section.

The fluorescence of the seed interior was also investigated for the 500 mg L^{-1} and 30-minute RITC-UMN and APTES-modified RITC-UMNs (Fig. S3†). The seed interior for RITC-UMNs (1085 ± 190 a.u.) positively correlated with the exterior of the seed (695 ± 35 a.u). The same was observed for APTES-modified RITC-UMNs that had a fluorescence of 385 ± 100 a.u. for the interior and 203 ± 65 a.u for the exterior. Since both treatments have similar trends for the fluorescence in the exterior and interior of the seeds, this suggests that results from the exterior of the seed, which is easier to image, can be used to draw general conclusions about cargo delivery into the interior of the seed, as well as the overall vacuum infiltration of RITC-UMNs. Since higher concentrations yield increased fluorescence and there was no difference in infiltration times, 500 mg L^{-1} of negatively-charged RITC UMNs with a 10-minute infiltration time was used for ongoing infiltration investigations.

Table 1 Range of optimization conditions tested for vacuum infiltration of RITC-UMNs

Condition	Range of condition values
Nanoparticle concentration	0, 125, 250, and 500 mg L^{-1}
Vacuum infiltration time	10, 20, and 30 minutes
Ionic salts	K_2SO_4, KNO_3, $MgSO_4$, and $Mg(NO_3)_2$
Ionic strength	40 and 200 mM
Seed pre-soaking time	0, 2, 4, 8, and 24 hours
pH	6, 6.5, 7, and 7.5

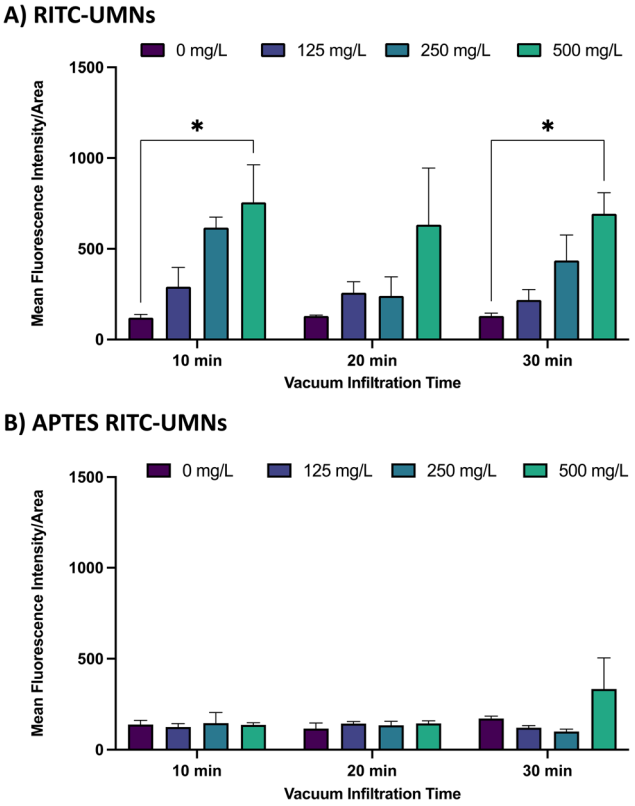

Fig. 5 Fluorescence intensities of (A) RITC-UMNs and (B) APTES RITC-UMNs at different nanoparticle concentrations (0, 125, 250 and 500 mg L^{-1}) and different infiltration times (10, 20, and 30 minutes). Error bars represent the standard error of three seed replicates. A two-way ANOVA with Tukey's multiple comparisons test was used to evaluate statistical significance (*$p < 0.05$).

Infiltration solution composition and ionic strength

Magnesium and potassium are essential macronutrients that promote plant health and growth, while sulfates and nitrates are incorporated into fertilizers to help soybeans meet their S and N requirements.[48] Changes in ionic strength of the NP-containing suspensions can also influence the uptake and transport of the suspension based on osmolarity gradients. To investigate the impact of different salts and ionic strength on RITC-UMN vacuum infiltration, RITC-UMN suspensions were prepared with ionic strengths of 40 mM and 200 mM using K_2SO_4, KNO_3, $MgSO_4$ and $Mg(NO_3)_2$. Additional suspensions for KNO_3 were prepared at 10 and 50 mM to have appropriate concentration comparisons since the KNO_3 ionic suspensions have the largest difference in concentrations when compared to the other treatments. Soybean seeds were also infiltrated with NP-free salt control solutions, and their fluorescence was comparable to the water controls, indicating that the K^+-based and Mg^{2+}-based salt treatments do not alter the auto-fluorescence of the soybean seeds (Fig. S4†).

For the seed exterior K^+-based salt RITC-UMN treatments (Fig. 6), the mean fluorescence signal was larger than the 500 mg L^{-1} RITC-UMN in water control treatment, with a statistically significant increase for the 50 mM KNO_3 treatment. The interior of the seed also showed increased fluorescence for K^+-based treatments, with greater fluorescence observed for higher ionic strengths. Contrary to the K^+-based salt RITC-UMN treatments, Mg^{2+}-based salt RITC-UMN treatments had reduced mean fluorescence for both the exterior and interior measurements (Fig. 6). We originally hypothesized that the increase in fluorescence observed for K^+-based treatments and decrease in fluorescence for Mg^{2+}-based treatments was due to the different concentrations of K^+ and Mg^{2+} inside the seed, resulting in preferential diffusion of K^+ ions and additional RITC-UMNs into the soybean seeds, with less diffusion into the seed for Mg^{2+}. However, the baseline K^+ and Mg^{2+} content in seeds infiltrated with water were measured by ICP-OES; the K^+ content (11 270 $\pm$ 718 ppm) was significantly higher than the Mg^{2+} content (2283 $\pm$ 87 ppm), indicating that diffusion is not the main driving force for the preferential uptake of K^+-based RITC-UMN solutions. Overall, these fluorescence measurements tell us that ionic strength alone does not impact uptake upon vacuum infiltration since matched ionic strengths of different salts have different impacts on the RITC-UMN infiltration, but that type of ion (K^+ *vs.* Mg^{2+}) contributes more to efficiency of nanoparticle infiltration.

Seed coat elemental content and nanoparticle stability

To complement the fluorescence-based infiltration data, the elemental content of relevant ions from the nanoparticles or infiltration solutions (*i.e.* silicon, potassium, magnesium and sulfur) in soybean seed coats were measured using ICP-OES. Although the seed has background concentrations of all of these nutrients, the silicon content is representative of the presence of either RITC-UMNs or APTES-modified RITC-UMNs, while potassium, magnesium and sulfur ions were tracked to account for co-infiltration of beneficial nutrients. Fig. 7a compares the silicon content and the mean fluorescence readout of soybean seed coats for negatively-charged RITC-UMNs and positively-charged APTES-modified RITC-UMNs. Compared to controls, both nanoparticles significantly increase the silicon content in the seed coat (Fig. S5a†). However, the negatively-charged nanoparticles have a significantly higher silicon content compared to the positively-charged nanoparticles, which aligns with the seed exterior fluorescence intensity measurements that also show a preference for the negatively-charged nanoparticles (Fig. 7a). This effect is due to differences in nanoparticle stability pre- and post-vacuum application and seed priming. More specifically, as seen in Fig. 8a and b, the hydrodynamic size of negatively-charged RITC-UMNs is unchanged before and after vacuum infiltration and seed priming; however, there is a significant increase in the hydrodynamic diameters of positively-charged APTES RITC-UMNs from 200.4 $\pm$ 3.31 nm to 4526 $\pm$ 395.6 nm (vacuum infiltration) and 200.4 $\pm$ 3.31 nm to 3068 $\pm$ 202.9 nm (seed priming). Vacuum infiltrations and seed priming applications also result in changes for the ζ-potential measurements as shown in Fig. 8c and d. In water, the RITC-UMNs have a ζ-potential of -46.86 ± 1.02 mV while the APTES RITC-UMNs have a ζ-potential of 26.03 $\pm$ 1.05 mV, which indicates that

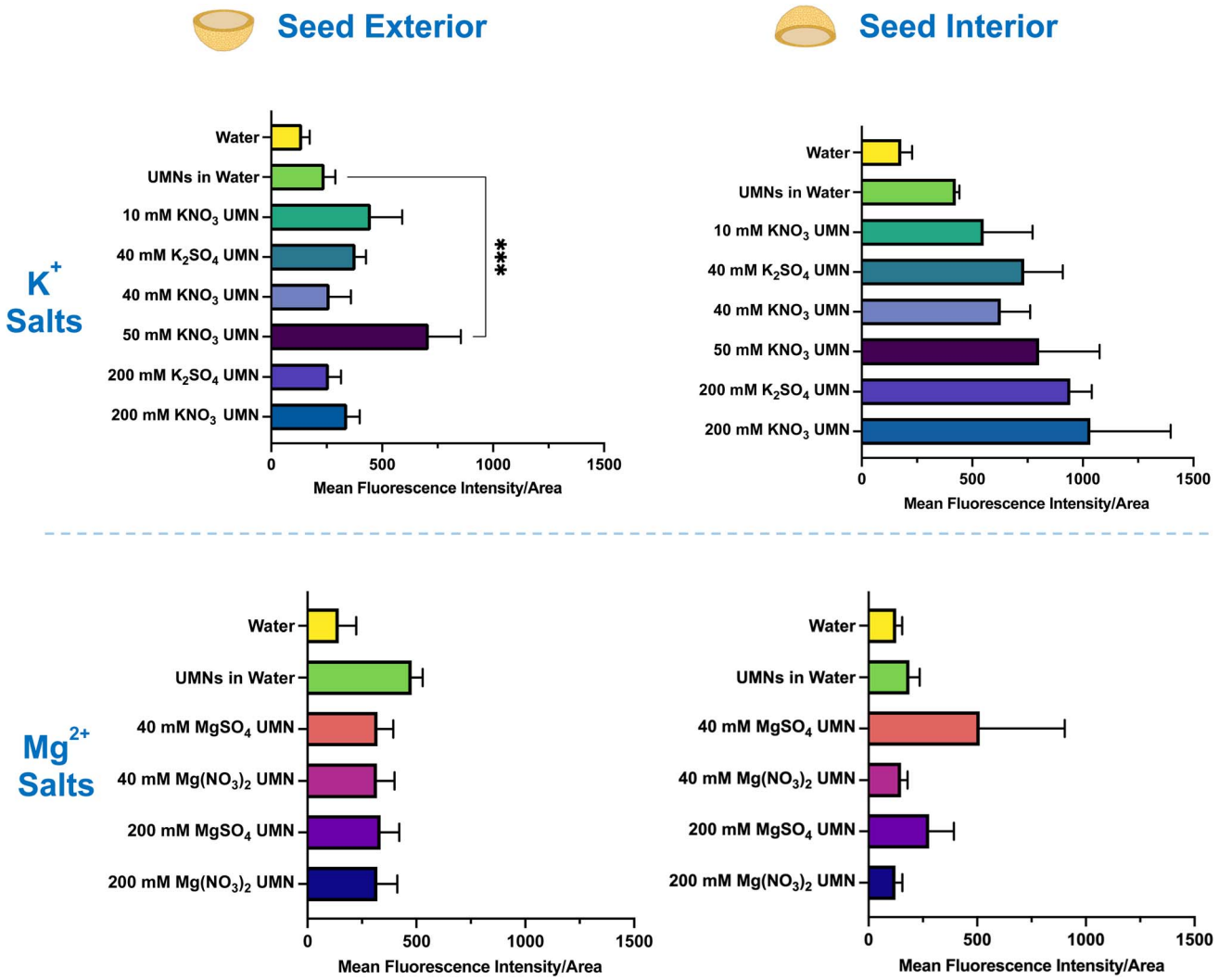

Fig. 6 Fluorescence intensities of 500 mg L^{-1} RITC-UMNs in K- and Mg-based salts with ionic strengths of 40 mM and 200 mM for both the seed exterior (left panel) and seed interior (right panel). 10 mM and 50 mM were included for KNO_3 as concentration comparisons. Error bars represent the standard error of three seed replicates. A one-way ANOVA with Dunnett's multiple comparisons test was used to evaluate statistical significance (***$p < 0.001$). Soybean icon created in https://www.biorender.com/.

both RITC-UMNs are more stable in the pre-infiltration conditions. Similar to the changes shown in size, the APTES-modfied RITC-UMNs show significant changes to the ζ-potential upon vacuum infiltration (reduced to -0.73 ± 0.32 mV) and conventional priming (reduced to 8.49 ± 0.68 mV). The RITC-UMNs also show changes in ζ-potential, but the values stay within the generally acceptable nanoparticle stability range of >|20| mV. These significant changes to nanoparticle characteristics and stability for the positively-charged nanoparticles explains the preferential accumulation of negatively-charged nanoparticles, which are smaller and more stable in solution. Additionally, these nanoparticles are in contact with biological systems that could result in the formation of a biomolecule coronas that can affect their size, stability, and overall uptake. The total protein content in the left-over vacuum infiltration and seed priming solutions was measured; there is a dose-dependent increase in the total amount of protein released into solution when seeds are placed in water (Fig. S6a†). Proteins were also detected in the treatment solutions in the presence of UMNs, although there is no surface charge-dependent difference (Fig. S6b†). The presence of protein indicates corona formation is likely and may play a role in nanoparticle uptake; however, further investigation of corona impact on vacuum infiltration is outside the scope of this paper and needs to be further studied.

The soybean seed coat silicon content of RITC-UMNs infiltrated with potassium- and magnesium-based ionic salt solutions at 200 mM is shown in Fig. 7b. Similar to water-based treatments, RITC-UMNs significantly increased silicon content (Fig. S5c and d†) compared to controls, but ion-specific differences were observed; importantly, these findings again align with the mean fluorescence intensity results (Fig. 6). For the sulfate counter ions at the same ionic strength (Fig. 7b), there is a statistically significant higher silicon content for K^+ (730 ± 39 ppm) compared to Mg^{2+} (486 ± 8 ppm). A similar trend is observed for the nitrate counter ions, although not statistically

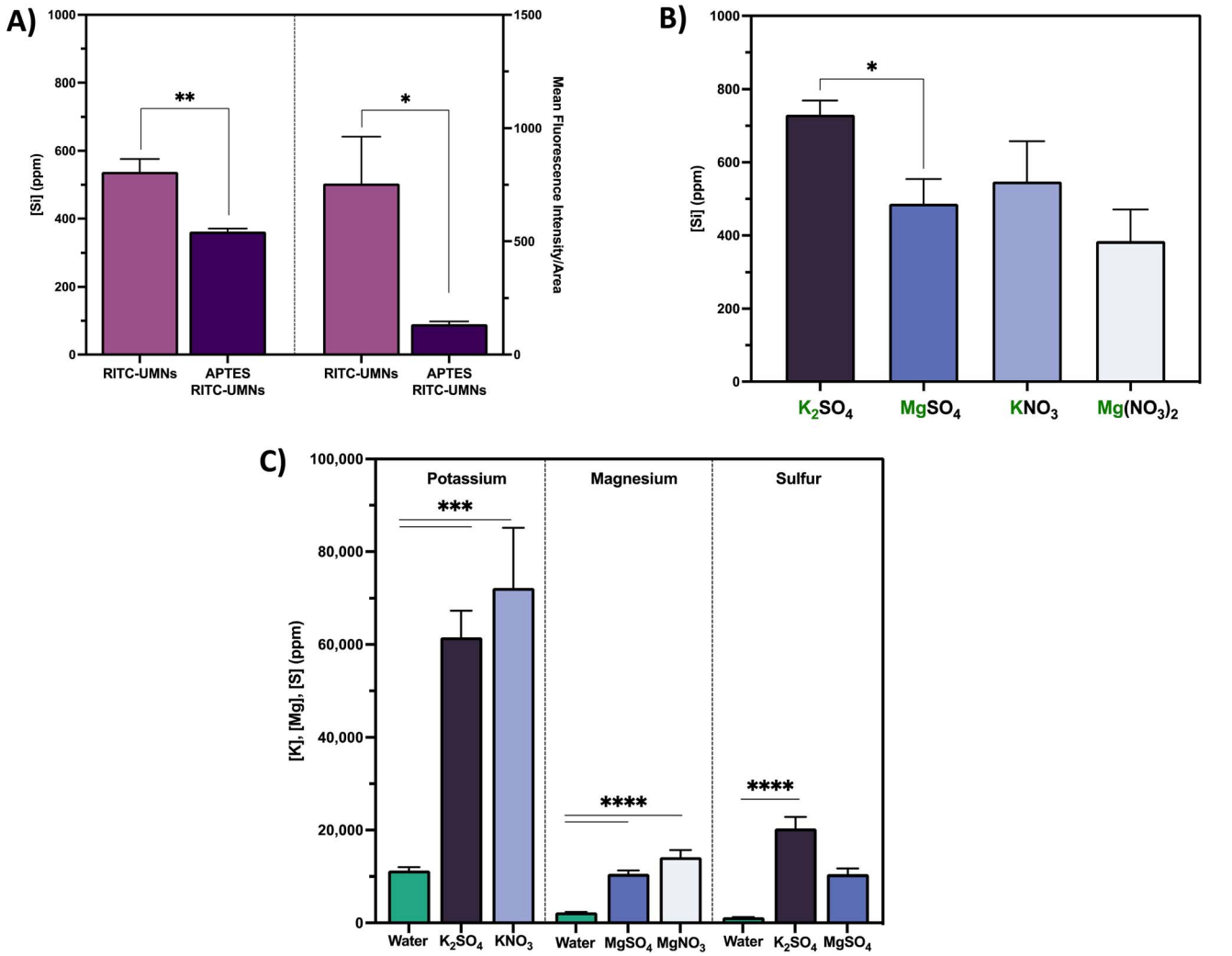

Fig. 7 (A) Silicon content of soybean seed coats (left) and seed exterior fluorescence intensity (right) of seeds infiltrated with negatively-charged RITC-UMNs and positively-charged APTES RITC-UMNs in water. (B) Silicon content of soybean seed coats infiltrated with RITC-UMNs in 200 mM K^+ and Mg^{2+} salt infiltrations. (C) Potassium, magnesium, and sulfur content in soybean seed coat infiltrated with RITC-UMNs in water, 200 mM K^+ and Mg^{2+} salt solutions. Error bars represent the standard error of triplicate measurements. An unpaired *t*-test, one-way ANOVA with Tukey's multiple comparisons test and one-way ANOVA with Dunnett's multiple comparisons test, respectively, were used to evaluate statistical significance ($*p < 0.05$, $**p < 0.01$, $***p < 0.001$, $****p < 0.0001$).

significant. Even at the lower ionic strength (50 mM KNO_3), K^+ (623 ± 127 ppm) resulted in a significantly higher silicon content when compared to Mg^{2+} (384 ± 86 ppm) at a higher ionic strength (200 mM $Mg(NO_3)_2$) (Fig. S5b†), further demonstrating the significant impact of ion-type (K^+ over Mg^{2+}) rather than ionic strength, which was previously observed for the fluorescence measurements (Fig. 6). Lastly, the benefits of using ionic salts as infiltration solutions are seen in Fig. 7c, where the beneficial nutrients potassium, magnesium, and sulfur are being co-delivered to the seed coat with the nanoparticle treatment. As expected, the vacuum infiltration of RITC-UMNs with ionic salts results in a statistically significant increase in potassium, magnesium, and sulfur content compared to the baseline content with water. Similar to the fluorescence measurements, there is a corresponding trend of greater potassium delivery from potassium salts compared to magnesium delivery from magnesium salts, likely due to the fact that magnesium ions are known to weakly bind to soybean seed coat cell walls.[49] Furthermore, soybeans are known to have high-affinity potassium transporters that can facilitate the preferential uptake in potassium-based solutions.[50] Given this added benefit of co-delivery and fortification of nutrients, future work will focus on greenhouse and field studies to measure downstream plant impacts of ionic salt infiltrations, including potential nano-enabled biofortification of crop edible tissues. By optimizing vacuum infiltration with varied ionic conditions, we were able to fortify soybean seeds with beneficial nutrients in addition to the nanoparticle treatment. This result shows the promise that changing the infiltration solution to include other agrochemicals, like pesticides, can enable pesticide delivery. Additionally, it would be interesting to explore the delivery of pesticide-loaded nanoparticles whereby the controlled, and

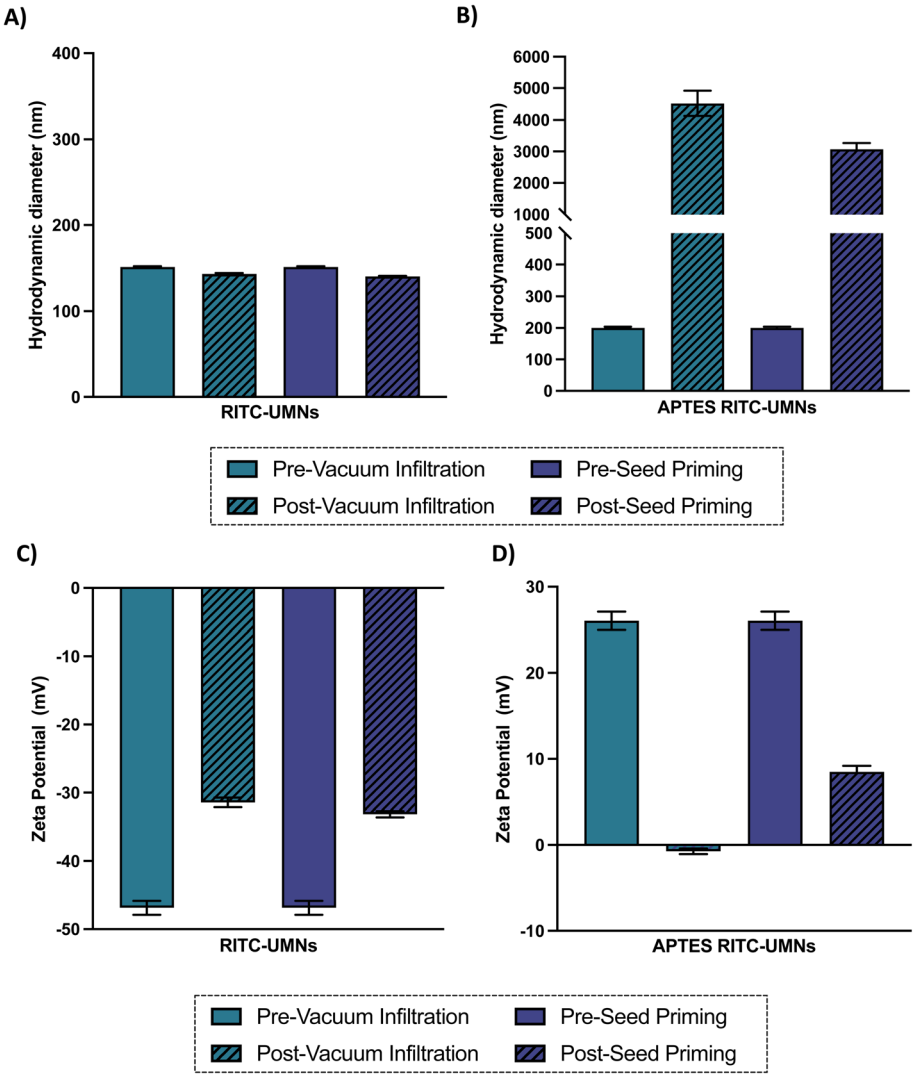

Fig. 8 Hydrodynamic diameter of (A) RITC-UMNs and (B) APTES RITC-UMNs in water before and after vacuum infiltration and seed priming. Zeta potential of (C) RITC-UMNs and (D) APTES RITC-UMNs in water before and after vacuum infiltration and seed priming. Error bars represent the standard deviation of three technical replicates. Note: Fig. 7b has a segmented *y*-axis to accurately represent differences in size.

long-term, release of pesticide can allow for crop protection across the growth cycle of the seeds. Overall, using seed treatments in tandem with nanoparticles may allow growers to use decreased field treatment inputs, facilitating precision delivery while maintaining, or improving, agricultural productivity.

Seed pre-soaking and solution pH

Presoaking of seeds was studied to investigate if coat softening would increase permeability and enable greater incorporation of vacuum infiltrated RITC-UMNs. However, seeds soaked in water for 2, 4, 8, and 12 hours showed no changes in mean fluorescence intensity (Fig. S7†), indicating that presoaking does not enable greater incorporation of RITC-UMNs onto the outside surface of the seeds. It is possible that presoaking the seeds in water saturated the outer portions of the seeds, thereby inhibiting uptake of more water and RITC-UMNs upon vacuum infiltration. Additionally, the impact of pH was studied using environmentally relevant pH values ranging from pH 6 to pH 7 as intracellular pH gradients may help drive suspension uptake. The RITC-UMN control suspensions (with no pH adjustments) that were used throughout these experiments had a pH of approximately 7. Compared to the fluorescence readout of the RITC-UMNs in water (757 ± 302 a.u.), there was a slight increase in the fluorescence of RITC-UMN suspensions with a pH of 6, 6.5 and 7.5, at 1003 ± 99 a.u., 1002 ± 147 a.u. and 1084 ± 261 a.u., respectively, although high replicate variability precluded statistical significance (Fig. S7†). The seed interior fluorescence was examined for RITC-UMNs with a pH of 7.5 since it had the largest exterior seed fluorescence. The seed interior fluorescence positively correlated with the exterior and produced larger fluorescence response with 1195 ± 400 a.u. and 1070 ± 535 a.u. for RITC-UMNs in water and adjusted pH to 7.5, respectively. While the seed interior fluorescence was greater, large variability precluded statistical significance between the interior and exterior of the seeds.

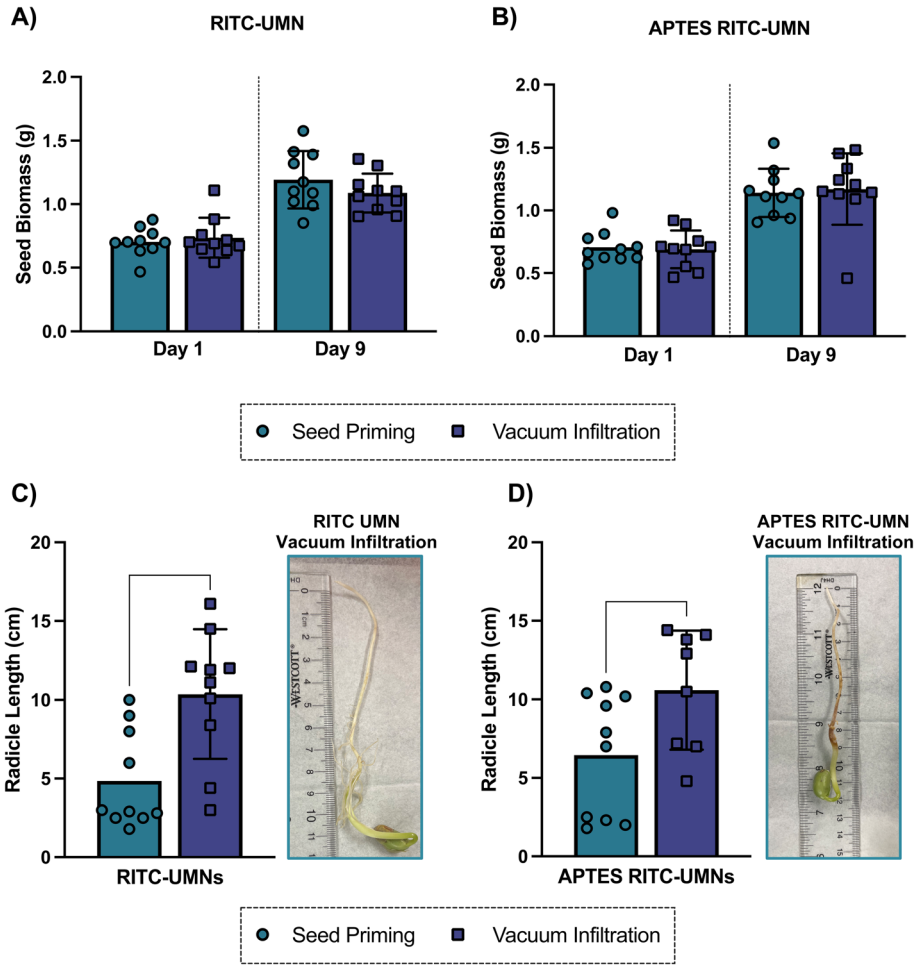

Fig. 9 Soybean seed biomass at the start and end of germinations for (A) RITC-UMNs and (B) APTES RITC-UMNs following seed priming and vacuum infiltration. Radicle length of soybean seeds was measured on day 9 for (C) RITC-UMNs and (D) APTES RITC-UMNs for both seed priming and vacuum infiltration. Images show radicle at the end of germination for vacuum infiltration for (C) RITC-UMNs & (D) APTES RITC-UMNs. Error bars represent the standard deviations of 10 seed replicates. Unpaired *t*-tests were used to evaluate statistical significance (**$p < 0.01$, *$p < 0.05$).

Impact of vacuum infiltration on soybean seed germination

The process of soaking seeds in a solution of interest without initiating germination, also known as seed priming, has long been used to enhance germination by facilitating more rapid initiation of radicle emergence and growth.[51,52] Some common priming strategies include hydropriming (water treatments), halopriming (salt solution treatments), hormopriming (hormone treatments), and more recently nanopriming (nanoparticle treatments).[9,51] The current work involves a modified seed priming method that includes a vacuum application; as such, a germination test was used to measure the resulting germination of seeds treated with infiltration salt treatments as well as negatively- and positively-charged UMNs at 500 mg L^{-1} with a 10-minute infiltration time (Fig. 9, S8 and S9†). The soybean seed biomass was measured over the course of 9 days post-application; there was no difference in biomass in the presence or absence of a vacuum application (Fig. 9a and b) for either nanoparticle type. This result was consistent over all days reported (Fig. S8†) and suggests that the application of vacuum does not negatively impact the quality of seeds that were germinated. However, the final radicle length, measured on the last day of germination and shown in Fig. 8c and d, highlights some benefits of vacuum application. For both negatively- and positively-charged nanoparticles, the radicle length was significantly longer in vacuum applied nanoparticles when compared to their no-vacuum counterparts. Seed priming treatments have been shown to promote root growth, especially in stress-induced conditions, due to the accelerated metabolism of primed seeds.[53] Here, the combination of the seed priming treatment with an external vacuum application seems to promote root development that would facilitate greater acquisition of nutrients from the soil, and later promote seedling development and establishment.

Conclusion

This is the first study to systematically investigate a novel vacuum infiltration-based seed treatment strategy that provides a simpler, safer and more targeted delivery method compared to in-field agrochemical applications. Nanoparticle surface charge

and concentration, infiltration time, seed presoaking, infiltrate ionic strength and pH, were investigated to optimize nanoscale nutrient loading *via* vacuum-infiltration based seed treatment. Higher nanoparticle concentrations at shorter infiltration times allow for more incorporation into the seed showing that infiltrations can be performed faster than previously reported without compromising performance. The enhanced incorporation of negatively-charged nanoparticles as demonstrated by both fluorescence and elemental content measurement was shown to be a function of changes to the stability and size of the positively-charged particles during infiltration and conventional priming. Enhanced nanoparticle delivery and nutrient fortification was achieved in potassium-based suspensions compared to magnesium due to high-affinity potassium transporters in soybean seeds. Future work will translate these optimized protocols to greenhouse and field studies and evaluate positive downstream plant impacts (*e.g.* enhanced nutrient fortification, biomass, disease suppression, gene expression). Since the presoaking treatments in water yielded no difference in fluorescence, subsequent experiments should examine the effect of presoaking seeds in nanoparticle suspensions prior to infiltration to evaluate additive or synergistic effects of combined novel and conventional seed treatments strategies. Additionally, since these nanoparticles are fluorescently labelled, the vacuum-infiltrated seeds can be used to understand the translocation and localization within soybean plants as they germinate and grow. Lastly, similar optimization conditions should be evaluated for other crop species and nanoparticle types, as well as with other agrochemicals, to diversify treatment options and enable commercialization. This work adds to a rapidly growing literature and field of research demonstrating that nano-enabled agriculture can be a safe and effective strategy to significantly increase food quality and production. The development and deployment of such strategies will be a foundational component of the necessary transformation of agriculture to combat global food insecurity in a changing climate.

Data availability

The data supporting this article have been included as part of the ESI.†

Author contributions

TLO, BT and CLH conceived the idea of this manuscript, designed experiments and supervised the project. TLO designed, synthesized, and characterized fluorescent nanoparticles, vacuum infiltrated seeds with nanoparticles, developed seed preparation for imaging, analyzed fluorescent images, prepared figures/graphs, performed statistical analysis, drafted and edited the manuscript. BT characterized nanoparticles, vacuum infiltrated seeds with nanoparticles, developed seed preparation for imaging, conducted spectral imaging and linear unmixing, designed seed elemental content experiments, conducted seed germination experiments, prepared graphs/figures, conducted statistical analysis, drafted and edited the manuscript. CD and JCW quantified seed elemental content. WHE performed initial vacuum infiltration experiments. SM synthesized and characterized fluorescent nanoparticles. RJ performed salt germination experiments. MAS assisted in sample preparation for seed images and image analysis.

Conflicts of interest

There are no conflicts to declare.

Acknowledgements

This work was supported by the National Science Foundation under Grant No. CHE-2001611, the NSF Center for Sustainable Nanotechnology. The CSN is part of the Centers for Chemical Innovation Program. The TEM imaging in this study was carried out in the Characterization Facility, University of Minnesota, which receives partial support from the National Science Foundation through the MRSEC program (award number DMR-2011401). Some figures and icons and graphical abstract were created in **https://www.biorender.com/**. B. S. T is supported by the University of Minnesota Interdisciplinary Doctoral Fellowship and Doctoral Dissertation Fellowship. S. M. acknowledges support from the Louis Stokes North Star STEM Alliance and the Louis Stokes Alliance for Minority Participation (NSF grant #1712629). This work was supported by the resources and staff at the University of Minnesota University Imaging Centers (UIC) SCR_020997. We want to acknowledge Dr Mary Brown and Dr Guillermo Marques for help with sample preparation, image acquisition, and image analysis expertise.

References

1 The State of Food Security and Nutrition in the World 2021. Transforming food systems for food security, improved nutrition and affordable healthy diets for all, FAO, IFAD, UNICEF, WFP and WHO, FAO, Rome, 2021.
2 M. Kah, N. Tufenkji and J. C. White, Nano-enabled strategies to enhance crop nutrition and protection, *Nat. Nanotechnol.*, 2019, **14**, 532–540.
3 X. Zhang, E. A. Davidson, D. L. Mauzerall, T. D. Searchinger, P. Dumas and Y. Shen, Managing nitrogen for sustainable development, *Nature*, 2015, **528**, 51–59.
4 P. S. Bindraban, C. O. Dimkpa, J. C. White, F. A. Franklin, A. Melse-Boonstra, N. Koele, R. Pandey, J. Rodenburg, K. Senthilkumar, P. Demokritou and S. Schmidt, Safeguarding human and planetary health demands a fertilizer sector transformation, *Plants People Planet*, 2020, **2**, 302–309.
5 M. W. Aktar, D. Sengupta and A. Chowdhury, Impact of pesticides use in agriculture: their benefits and hazards, *Interdiscip. Toxicol.*, 2009, **2**, 1–12.
6 D. Pimentel, Environmental and Economic Costs of the Application of Pesticides Primarily in the United States, *Environ. Dev. Sustainability*, 2005, **7**, 229–252.

7 D. Coskun, D. T. Britto, W. Shi and H. J. Kronzucker, Nitrogen transformations in modern agriculture and the role of biological nitrification inhibition, *Nat. Plants*, 2017, **3**, 17074.
8 C. O. Dimkpa, J. Fugice, U. Singh and T. D. Lewis, Development of fertilizers for enhanced nitrogen use efficiency - Trends and perspectives, *Sci. Total Environ.*, 2020, **731**, 139113.
9 S. Paparella, S. S. Araújo, G. Rossi, M. Wijayasinghe, D. Carbonera and A. Balestrazzi, Seed priming: state of the art and new perspectives, *Plant Cell Rep.*, 2015, **34**, 1281–1293.
10 B. Adhikari, P. R. Dhital, S. Ranabhat and H. Poudel, Effect of seed hydro-priming durations on germination and seedling growth of bitter gourd (*Momordica charantia*), *PLoS One*, 2021, **16**, e0255258.
11 M. A. Mir, R. John, M. N. Alyemeni, P. Alam and P. Ahmad, Jasmonic acid ameliorates alkaline stress by improving growth performance, ascorbate glutathione cycle and glyoxylase system in maize seedlings, *Sci. Rep.*, 2018, **8**, 2831.
12 T. Tabassum, M. Farooq, R. Ahmad, A. Zohaib and A. Wahid, Seed priming and transgenerational drought memory improves tolerance against salt stress in bread wheat, *Plant Physiol. Biochem.*, 2017, **118**, 362–369.
13 A. Saed-Moocheshi, A. Shekoofa, H. Sadeghi and M. Pessarakli, Drought and Salt Stress Mitigation by Seed Priming with KNO_3 and Urea in Various Maize Hybrids: An Experimental Approach Based on Enhancing Antioxidant Responses, *J. Plant Nutr.*, 2014, **37**, 674–689.
14 R. A. Khan, Response of Wheat (*Triticum aestivum* L.) to Zinc Sulphate and Copper Sulphate under Salt Stress, *Pure Appl. Biol.*, 2020, **9**, 2648–2658.
15 M. S. Saddiq, S. Iqbal, I. Afzal, A. M. H. Ibrahim, M. A. Bakhtavar, M. B. Hafeez, Jahanzaib and M. M. Maqbool, Mitigation of salinity stress in wheat (*Triticum aestivum* L.) seedlings through physiological seed enhancements, *J. Plant Nutr.*, 2019, **42**, 1192–1204.
16 M. A. Al-Mudaris and S. C. Jutzi, The Influence of Fertilizer-based Seed Priming Treatments on Emergence and Seedling Growth of Sorghum bicolor and Pennisetum glaucum in Pot Trials under Greenhouse Conditions, *J. Agron. Crop Sci.*, 2001, **182**, 135–142.
17 S. Paul, S. Dey and R. Kundu, Seed priming: an emerging tool towards sustainable agriculture, *Plant Growth Regul.*, 2021, **97**, 215–234.
18 S. H. Nile, M. Thiruvengadam, Y. Wang, R. Samynathan, M. A. Shariati, M. Rebezov, A. Nile, M. Sun, B. Venkidasamy, J. Xiao and G. Kai, Nano-priming as emerging seed priming technology for sustainable agriculture-recent developments and future perspectives, *J. Nanobiotechnol.*, 2022, **20**, 254.
19 R. De La Torre-Roche, J. Cantu, C. Tamez, N. Zuverza-Mena, H. Hamdi, I. O. Adisa, W. Elmer, J. Gardea-Torresdey and J. C. White, Seed Biofortification by Engineered Nanomaterials: A Pathway To Alleviate Malnutrition?, *J. Agric. Food Chem.*, 2020, **68**, 12189–12202.
20 M. Sohail, T. Pirzada, C. H. Opperman and S. A. Khan, Recent advances in seed coating technologies: transitioning toward sustainable agriculture, *Green Chem.*, 2022, **24**, 6052–6085.
21 L. Abeywardana, M. de Silva, C. Sandaruwan, D. Dahanayake, G. Priyadarshana, S. Chathurika, V. Karunaratne and N. Kottegoda, Zinc-Doped Hydroxyapatite–Urea Nanoseed Coating as an Efficient Macro–Micro Plant Nutrient Delivery Agent, *ACS Agric. Sci. Technol.*, 2021, **1**, 230–239.
22 Z. Elhaj Baddar and J. M. Unrine, Effects of Soil pH and Coatings on the Efficacy of Polymer coated ZnO Nanoparticle fertilizers in Wheat (*Triticum aestivum*), *Environ. Sci. Technol.*, 2021, **55**, 13532–13540.
23 T. Xu, C. Ma, Z. Aytac, X. Hu, K. W. Ng, J. C. White and P. Demokritou, Enhancing Agrichemical Delivery and Seedling Development with Biodegradable, Tunable, Biopolymer-Based Nanofiber Seed Coatings, *ACS Sustain. Chem. Eng.*, 2020, **8**, 9537–9548.
24 FAO, Agricultural production statistics (2000-2021), 2022.
25 M. Li, L. Gao, J. C. White, C. L. Haynes, T. L. O'Keefe, Y. Rui, S. Ullah, Z. Guo, I. Lynch and P. Zhang, Nano-enabled strategies to enhance biological nitrogen fixation, *Nat. Nanotechnol.*, 2023, **18**, 688–691.
26 C. A. O'Bryan, K. Kushwaha, D. Babu, P. G. Crandall, M. L. Davis, P. Chen, S.-O. Lee and S. C. Ricke, Soybean Seed Coats: A Source of Ingredients for Potential Human Health Benefits-A Review of the Literature, *J. Food Res.*, 2014, **3**, 188.
27 L. Sun and Z. Yuan, in *Soybean Physiology and Genetics*, 2022, pp. 349–375, DOI: **10.1016/bs.abr.2022.03.004**.
28 D. Qutob, F. Ma, C. A. Peterson, M. A. Bernards and M. Gijzen, Structural and permeability properties of the soybean seed coat, *Botany*, 2008, **86**, 219–227.
29 W. Elmer and J. C. White, The Future of Nanotechnology in Plant Pathology, *Annu. Rev. Phytopathol.*, 2018, **56**, 111–133.
30 S. M. Rodrigues, P. Demokritou, N. Dokoozlian, C. O. Hendren, B. Karn, M. S. Mauter, O. A. Sadik, M. Safarpour, J. M. Unrine, J. Viers, P. Welle, J. C. White, M. R. Wiesner and G. V. Lowry, Nanotechnology for sustainable food production: promising opportunities and scientific challenges, *Environ. Sci.: Nano*, 2017, **4**, 767–781.
31 P. Wang, E. Lombi, F.-J. Zhao and P. M. Kopittke, Nanotechnology: A New Opportunity in Plant Sciences, *Trends Plant Sci.*, 2016, **21**, 699–712.
32 P. Hu, J. An, M. M. Faulkner, H. Wu, Z. Li, X. Tian and J. P. Giraldo, Nanoparticle Charge and Size Control Foliar Delivery Efficiency to Plant Cells and Organelles, *ACS Nano*, 2020, **14**, 7970–7986.
33 J. Borgatta, C. Ma, N. Hudson-Smith, W. Elmer, C. D. Plaza Pérez, R. De La Torre-Roche, N. Zuverza-Mena, C. L. Haynes, J. C. White and R. J. Hamers, Copper Based Nanomaterials Suppress Root Fungal Disease in Watermelon (*Citrullus lanatus*): Role of Particle Morphology, Composition and Dissolution Behavior, *ACS Sustain. Chem. Eng.*, 2018, **6**, 14847–14856.

34 J. T. Buchman, W. H. Elmer, C. Ma, K. M. Landy, J. C. White and C. L. Haynes, Chitosan-Coated Mesoporous Silica Nanoparticle Treatment of *Citrullus lanatus* (Watermelon): Enhanced Fungal Disease Suppression and Modulated Expression of Stress-Related Genes, *ACS Sustain. Chem. Eng.*, 2019, **7**, 19649–19659.

35 H. Kang, J. Lee, T. O'Keefe, B. Tuga, C. J. Hogan Jr and C. L. Haynes, Effect of (3-aminopropyl)triethoxysilane on dissolution of silica nanoparticles synthesized *via* reverse micro emulsion, *Nanoscale*, 2022, **14**, 9021–9030.

36 H. Kang, W. Elmer, Y. Shen, N. Zuverza-Mena, C. Ma, P. Botella, J. C. White and C. L. Haynes, Silica nanoparticle dissolution rate controls the suppression of Fusarium wilt of watermelon (*Citrullus lanatus*), *Environ. Sci. Technol.*, 2021, **55**, 13513–13522.

37 B. Tuga, T. O'Keefe, C. Deng, A. T. Ligocki, J. C. White and C. L. Haynes, Designing nanoparticles for sustainable agricultural applications, *Trends Chem.*, 2023, **5**, 814–826.

38 A. Rastogi, D. K. Tripathi, S. Yadav, D. K. Chauhan, M. Zivcak, M. Ghorbanpour, N. I. El-Sheery and M. Brestic, Application of silicon nanoparticles in agriculture, *3 Biotech*, 2019, **9**, 90.

39 J. A. Bhat, N. Rajora, G. Raturi, S. Sharma, P. Dhiman, S. Sanand, S. M. Shivaraj, H. Sonah and R. Deshmukh, Silicon nanoparticles (SiNPs) in sustainable agriculture: major emphasis on the practicality, efficacy and concerns, *Nanoscale Adv.*, 2021, **3**, 4019–4028.

40 T. L. O'Keefe, C. Deng, Y. Wang, S. Mohamud, A. Torres-Gómez, B. Tuga, C.-H. Huang, W. R. Alvarez Reyes, J. C. White and C. L. Haynes, Chitosan-Coated Mesoporous Silica Nanoparticles for Suppression of *Fusarium virguliforme* in Soybeans (*Glycine max*), *ACS Agric. Sci. Technol.*, 2024, **4**, 580–592.

41 Y.-S. Lin and C. L. Haynes, Synthesis and Characterization of Biocompatible and Size-Tunable Multifunctional Porous Silica Nanoparticles, *Chem. Mater.*, 2009, **21**, 3979–3986.

42 S. M. Egger, K. R. Hurley, A. Datt, G. Swindlehurst and C. L. Haynes, Ultraporous Mesostructured Silica Nanoparticles, *Chem. Mater.*, 2015, **27**, 3193–3196.

43 N. A. Levan, A. S. Goggi and R. Mullen, Improving the Reproducibility of Soybean Standard Germination Test, *Crop Sci.*, 2008, **48**, 1933–1940.

44 Y. Wang, Z. Li, W. Zhong, H. Li, D. Xu and H. Chen, Rhodamine B doped silica nanoparticle labels for protein microarray detection, *Sci. China:Chem.*, 2010, **53**, 747–751.

45 P. Acharya, G. K. Jayaprakasha, K. M. Crosby, J. L. Jifon and B. S. Patil, Nanoparticle-Mediated Seed Priming Improves Germination, Growth, Yield, and Quality of Watermelons (*Citrullus lanatus*) at multi-locations in Texas, *Sci. Rep.*, 2020, **10**, 5037.

46 E. Spielman-Sun, E. Lombi, E. Donner, D. Howard, J. M. Unrine and G. V. Lowry, Impact of Surface Charge on Cerium Oxide Nanoparticle Uptake and Translocation by Wheat (*Triticum aestivum*), *Environ. Sci. Technol.*, 2017, **51**, 7361–7368.

47 E. Spielman-Sun, A. Avellan, G. D. Bland, R. V. Tappero, A. S. Acerbo, J. M. Unrine, J. P. Giraldo and G. V. Lowry, Nanoparticle surface charge influences translocation and leaf distribution in vascular plants with contrasting anatomy, *Environ. Sci.: Nano*, 2019, **6**, 2508–2519.

48 T. C. de Bang, S. Husted, K. H. Laursen, D. P. Persson and J. K. Schjoerring, The molecular-physiological functions of mineral macronutrients and their consequences for deficiency symptoms in plants, *New Phytol.*, 2021, **229**, 2446–2469.

49 J. A. Laszlo, Mineral contents of soybean seed coats and embryos during development, *J. Plant Nutr.*, 1990, **13**, 231–248.

50 M. Chao, L. Li, J. Zhang, L. Huang, R. Ren, X. Xu and Z. Huang, Structural features and expression regulation analysis of potassium transporter gene GmHAK5 in soybean (*Glycine max* L.), *Plant Growth Regul.*, 2023, **102**, 471–483.

51 A. Pagano, A. Macovei and A. Balestrazzi, Molecular dynamics of seed priming at the crossroads between basic and applied research, *Plant Cell Rep.*, 2023, **42**, 657–688.

52 J. D. Bewley, K. J. Bradford, H. W. M. Hilhorst and H. Nonogaki, in *Seeds: Physiology of Development, Germination and Dormancy*, ed. J. D. Bewley, K. J. Bradford, H. W. M. Hilhorst and H. Nonogaki, Springer New York, New York, NY, 3rd edn, 2013, pp. 133–181, DOI: **10.1007/978-1-4614-4693-4_4**.

53 C. Patanè, V. Cavallaro and S. L. Cosentino, Germination and radicle growth in unprimed and primed seeds of sweet sorghum as affected by reduced water potential in NaCl at different temperatures, *Ind. Crops Prod.*, 2009, **30**, 1–8.